

# Evolution in off-critical diblock copolymer melts

Michael Helmers\*   Barbara Niethammer\*   Xiaofeng Ren†

## Abstract

We study the evolution of diblock copolymer melts in which one component has small volume fraction. In this case one observes phase morphologies which consist of small spheres of the minority component embedded in the other component. Based on the Ohta-Kawasaki free energy one can set up an evolution equation which has the interpretation of a gradient flow. We restrict this gradient flow to morphologies in which the minority phase consists of spheres and derive monopole approximations for different parameter regimes. We use these approximations for simulations of large particle systems.

## 1 Introduction

### 1.1 Diblock copolymers

A diblock copolymer molecule is a linear sub-chain of  $N_A$   $A$ -monomers grafted covalently to another sub-chain of  $N_B$   $B$ -monomers. Because of the repulsion between the unlike monomers, the different type sub-chains tend to segregate, but as they are chemically bonded in chain molecules, segregation of sub-chains cannot lead to a macroscopic phase separation. Only a local micro-phase separation occurs: micro-domains rich in  $A$  and  $B$  emerge. These micro-domains form morphology patterns on a larger scale. In this paper we are mainly interested in the case that the fraction of, say,  $A$ -monomers in a chain is small. Then we observe patterns which consist of many small separated spheres rich in  $A$ -monomers.

### 1.2 The Ohta-Kawasaki free energy

The Ohta-Kawasaki [11] free energy of an incompressible diblock copolymer melt is a functional of the  $A$ -monomer density field. Let  $u(x)$  be the relative  $A$ -monomer number density at point  $x$  in the sample. When there is high  $A$ -monomer concentration at  $x$ ,  $u(x)$  is close to 1; when there is high concentration of  $B$ -monomers at  $x$ ,  $u(x)$  is close

---

\*Mathematical Institute, University of Oxford, 24-29 St. Giles', Oxford, OX1 3LB, UK

†Department of Mathematics and Statistics, Utah State University, Logan, UT 84322-3900, USA.

to 0. A value of  $u(x)$  between 0 and 1 means that a mixture of  $A$ - and  $B$ -monomers occupies  $x$ . The free energy of the system is written as

$$I_\eta(u) := \int_D \left( \frac{\eta}{2} |\nabla u|^2 + \frac{1}{\eta} W(u) + \frac{\gamma}{2} |(-\Delta)^{-1/2}(u - \rho)|^2 \right) dx, \quad (1)$$

defined in  $X_a = \{u \in W^{1,2}(D) : \bar{u} = \rho\}$ , where  $\bar{u} := \frac{1}{|D|} \int_D u$  is the average of  $u$  on  $D$ . When the free energy  $I_\eta$  is minimized, the three terms of the integrand (the energy density of the material) have different preferences. The first term likes large blocks of monomers, thereby reducing the total size of interfaces between the two monomers. The function  $W$  in the second term is a double well potential with two global minima at 0 and 1, reflecting its preference for segregated monomers over mixtures. The third nonlocal term is minimized if  $u \equiv \rho$ . However this configuration of  $u$  makes the second term large. The second best choice for the third term is to have  $u$  oscillate rapidly around  $\rho$ . This way, because of the compact nature of  $(-\Delta)^{-1/2}$  (when  $D$  is bounded),  $(-\Delta)^{-1/2}(u - \rho)$  becomes close to 0 and hence the third term becomes small. As these preferences compete and compromise, small blocks rich in  $A$ -monomers and  $B$ -monomers appear. This phenomenon is known as micro-phase separation. For a further analysis of the scaling of the energy we refer to [4].

### 1.3 The sharp interface limit

If  $\eta$  is small the interfacial regions become smaller and one can replace  $I_\eta$  by its sharp interface limit. In [10] the Ohta-Kawasaki theory is formulated on a bounded domain as a singularly perturbed variational problem with a nonlocal term and the limiting sharp interface problem is identified. The latter is rigorously derived in [12] as a  $\Gamma$ -limit of the singularly perturbed variational problem.

In this paper we consider an idealized situation, in which  $D = \mathbb{R}^3$ , so we formulate the energy directly for this case. The corresponding energy is defined for all  $\Omega \in \mathbb{R}^3$  with  $|\Omega| = \rho$  and is given by

$$E(\Omega) = \mathcal{H}^2(\partial\Omega) + \frac{\gamma}{2} \int_{\mathbb{R}^3} |(-\Delta)^{-1/2}\chi|^2 dx, \quad (2)$$

where  $\chi$  is the characteristic function of  $\Omega$  and  $\int_{\mathbb{R}^3} |(-\Delta)^{-1/2}\chi|^2 dx = \int_{\mathbb{R}^3} |\nabla\mu|^2 dx$  with  $-\Delta\mu = \chi$  in  $\mathbb{R}^3$ .

### 1.4 A time dependent model

We are interested in how an initial configuration of a diblock copolymer melt evolves towards a state of minimal energy. An appropriate evolutionary model set in whole space which reduces  $E$  and keeps the volume fraction of both phases conserved is the

following Mullins-Sekerka type free boundary problem. In this model the normal velocity  $v$  of the interface  $\partial\Omega = \partial\Omega(t)$  is given by

$$v = [\nabla u \cdot \vec{n}] \quad \text{on } \partial\Omega, \quad (3)$$

where  $[\nabla u \cdot \vec{n}]$  denotes the jump of the normal component of the gradient across the interface. (Here  $\vec{n}$  denotes the outer normal to  $\Omega$  and  $[f] = \lim_{x \notin \Omega, x \rightarrow \partial\Omega} f(x) - \lim_{x \in \Omega, x \rightarrow \partial\Omega} f(x)$ .) The potential  $u$  is for each time determined via

$$-\Delta u = 0 \quad \text{in } \mathbb{R}^3 \setminus \partial\Omega, \quad (4)$$

$$u = \kappa + \gamma(-\Delta)^{-1}\chi \quad \text{on } \partial\Omega \quad (5)$$

with no-flux boundary conditions for  $u$  at infinity. Aspects of a local well-posedness theory for the Mullins-Sekerka-model (that is the case  $\gamma = 0$ ) can be found for example in [2], [3] and [6].

### 1.5 The gradient flow structure of the evolutionary model

The evolution defined by (3)-(5) has an interpretation as a gradient flow on a Riemannian manifold, more precisely it is the gradient flow of the energy (2) with respect to the  $H^{-1}$  norm in the bulk. To reveal this structure consider the manifold of subsets of  $\mathbb{R}^3$  with fixed volume, that is  $\mathcal{M} := \{\Omega \subset \mathbb{R}^3 \mid |\Omega| = \rho\}$ . The tangent space  $T_\Omega \mathcal{M}$  at an element  $\Omega \in \mathcal{M}$  is described by all kinematically admissible normal velocities of  $\partial\Omega$ , that is,

$$T_\Omega \mathcal{M} = \left\{ v: \partial\Omega \rightarrow \mathbb{R} \mid \int_{\partial\Omega} v dS = 0 \right\}.$$

The metric tensor on the tangent space is given by the  $H^{-1}$  norm, that is

$$g_\Omega(v^1, v^2) = \int_{\mathbb{R}^3} \nabla u^1 \cdot \nabla u^2 dx, \quad (6)$$

where  $u^\alpha$  solves

$$\begin{aligned} -\Delta u^\alpha &= 0 & \text{in } \mathbb{R}^3 \setminus \partial\Omega, \\ [\nabla u^\alpha \cdot \vec{n}] &= v^\alpha & \text{on } \partial\Omega. \end{aligned} \quad (7)$$

Notice, that  $u$  is well-defined up to an additive constant (see also [5] for a rigorous set-up). The gradient flow of the energy (2) is now the dynamical system where at each time the velocity is the element of the tangent space which points in the direction of steepest descent of the energy. In other words,  $v$  is such that

$$g_{\Omega(t)}(v, \tilde{v}) = -\langle DE(\Omega(t)), \tilde{v} \rangle \quad (8)$$

for all  $\tilde{v} \in T_{\Omega(t)} \mathcal{M}$ . Choosing  $\tilde{v} = v$  we immediately obtain the energy estimate associated with each gradient flow, which is

$$\int_0^T g_{\Omega(t)}(v, v) dt + E(\Omega(T)) = E(\Omega(0)) \quad (9)$$

for all  $T > 0$ .

It is well known that the first variation of the surface energy, the first summand of  $E$ , is the mean curvature. The second nonlocal part is given by  $\int_{\mathbb{R}^3} |\nabla \mu|^2 dx$ , where  $\mu$  solves  $-\Delta \mu = \chi$ . Hence  $\int_{\mathbb{R}^3} |\nabla \mu|^2 dx = \int_{\mathbb{R}^3} \mu \chi dx = \int_{\Omega} \mu dx$  and the first variation in direction  $\tilde{v} \in T_{\Omega} \mathcal{M}$  is given by  $\int_{\partial \Omega} \mu \tilde{v} dS$ . Thus (8) reads after an integration by parts in the metric tensor

$$\int_{\partial \Omega} u \tilde{v} dS = \int_{\partial \Omega} (\kappa + \gamma \mu) \tilde{v} dS \quad (10)$$

for all  $\tilde{v} \in T_{\Omega(t)} \mathcal{M}$ , which is up to an irrelevant constant just (5).

The advantage of the gradient flow perspective is that it can be restricted in a natural way to a lower dimensional submanifold. We will make use of this idea in the next section.

## 2 Reduced models

### 2.1 Off-critical mixtures and restriction to spherical particles

In the following we are interested in the regime where the fraction of  $A$ -monomers is much smaller than the one of  $B$ -monomers. In this case the  $A$ -phase consists of a set of many small disconnected approximately spherical particles. In view of this fact it seems natural to restrict the evolution (3)-(5) to spherical particles by restricting the gradient flow to such morphologies. For the case  $\gamma = 0$  it has been shown rigorously in [1] that such an approximation is valid. We also refer to [13], in which stable states to the energy are established which consist of a collection of spheres.

We define the submanifold  $\mathcal{N} \subset \mathcal{M}$  which consists of all sets  $\Omega$  which are the union of disjoint balls

$$\Omega = \cup_i B_{R_i}(X_i),$$

where the centers  $\{X_i\}_i$  and the radii  $\{R_i\}_i$  are variable. Hence  $\mathcal{N}$  can be identified with an open subspace of the hypersurface  $\{\mathbf{Y} = \{R_i, X_i\}_i \in \mathbb{R}_+ \times \mathbb{R}^3 \mid \frac{4\pi}{3} \sum_i R_i^3 = \rho\}$  in  $\mathbb{R}^{4N}$ , where  $N$  is the number and  $i = 1, \dots, N$  an enumeration of the particles. The tangent space can be identified with the hyperplane

$$T_{\mathbf{Y}} \mathcal{N} = \{\mathbf{Z} = \{V_i, \xi_i\}_i \in \mathbb{R} \times \mathbb{R}^3 \mid \sum_i R_i^2 V_i = 0\} \subset \mathbb{R}^{4N},$$

such that  $V_i$  describes the rate of change of the radius of particle  $i$  and  $\xi_i$  the rate of change of its center.

The restriction of the metric tensor can be expressed as

$$g_{\mathbf{Y}}(\mathbf{Z}^1, \mathbf{Z}^2) = \int_{\mathbb{R}^3} \nabla w^1 \cdot \nabla w^2 dx,$$

where the function  $w^\alpha$  solves

$$\begin{aligned} -\Delta w^\alpha &= 0 && \text{in } \mathbb{R}^3 \setminus \cup_i \partial B_{R_i}(X_i), \\ [\nabla w^\alpha \cdot \vec{n}] &= V_i^\alpha + \xi_i^\alpha \cdot \vec{n} && \text{on } \partial B_{R_i}(X_i). \end{aligned} \quad (11)$$

For the following it will be convenient to split the metric tensor into the radial and shift part respectively. We write

$$w = u + \phi$$

where  $u$  and  $\phi$  are harmonic in- and outside the particles and where

$$\begin{aligned} [\nabla u \cdot \vec{n}] &= V_i && \text{on } \partial B_{R_i}(X_i), \\ [\nabla \phi \cdot \vec{n}] &= \xi_i \cdot \vec{n} && \text{on } \partial B_{R_i}(X_i). \end{aligned} \quad (12)$$

It turns out to be notationally convenient to consider the normalized energy  $E = E_{surf} + \gamma E_{nl}$ , where

$$E_{surf} = \frac{1}{2} \mathcal{H}^2(\partial\Omega) = 4\pi \sum_i \frac{R_i^2}{2}$$

and

$$E_{nl} = \frac{3}{2} \int_{\mathbb{R}^3} |\nabla \mu|^2 dx = \frac{3}{2} \sum_i \int_{B_{R_i}(X_i)} \mu dx$$

with  $\mu = -\Delta^{-1} \chi_{\cup B_{R_i}}$ . We obtain the differentials of the energies in the direction of a tangent vector  $\tilde{\mathbf{Z}} = \{\tilde{V}_i, \tilde{\xi}_i\}_i$  as

$$\langle DE_{surf}, \tilde{\mathbf{Z}} \rangle = 4\pi \sum_i R_i \tilde{V}_i \quad \text{and} \quad \langle DE_{nl}, \tilde{\mathbf{Z}} \rangle = \frac{3}{2} \sum_i \int_{\partial B_{R_i}(X_i)} \mu (\tilde{V}_i + \tilde{\xi}_i \cdot \vec{n}) dS.$$

We will see in Section 2.2 that also  $\langle DE_{nl}, \tilde{\mathbf{Z}} \rangle$  can be expressed explicitly in  $\{R_i, X_i\}_i$ . For the moment we just state once more the gradient flow equation. For any  $t \geq 0$  we chose  $\mathbf{Z}(t)$  such that

$$g_{\mathbf{Y}}(\mathbf{Z}, \tilde{\mathbf{Z}}) = -\langle DE, \tilde{\mathbf{Z}} \rangle = -4\pi \sum_i R_i \tilde{V}_i - \gamma \frac{3}{2} \sum_i \int_{\partial B_{R_i}(X_i)} \mu (\tilde{V}_i + \tilde{\xi}_i \cdot \vec{n}) dS \quad (13)$$

for all  $\tilde{\mathbf{Z}} \in T_{\mathbf{Y}}\mathcal{N}$ . We can expect that if initial data  $\{R_i(0), X_i(0)\}$  are given such that particles do not overlap, a smooth solution to (13) exists at least for short times. If a particle disappears the evolution is not smooth; however, we can extend continuously the solution by just starting again with the new configuration. Our evolution cannot be further extended when two or more particles collide. We cannot completely exclude such an event a priori. However, as we will see below, one part of the nonlocal energy is given by  $\sum_i \sum_{j \neq i} \frac{R_i^3 R_j^3}{|X_i - X_j|}$ , which again shows that this part of the energy prefers uniformly distributed particles. If the energy is initially bounded, it remains bounded for all times as long as a solution exists. Hence, centers  $X_i$  and  $X_j$  cannot come arbitrarily close unless the particles become very small at the same time. In particular our monopole approximation, which we will derive in Section 2.2 below, will be defined for all times. In the next Section 2.2 we solve the gradient flow equation. The main idea is that we can solve the equations for the potentials by superposition of suitable monopoles. We

will see, that the leading order terms in the equations differ, depending on whether the domain covered by the particles is larger or smaller than the well-known screening length that describes the effective interaction range of particles. In Section 2.3 we state the approximate equations for the gradient flow, first in the simplest case, where the screening length is much larger than the system size, and second in the case in which the system size is of the order of the screening length. Those equations are the starting point for our numerical simulations. In Section 2.4 we derive the corresponding mean-field models which arise if one passes to a description with densities and in Section 3 we identify stationary states. Finally, in Section 4 we present results of numerical simulations of the monopole approximation.

## 2.2 Solution by monopoles

In this section we almost explicitly give the solution of the gradient flow equation which is based on the fact that we can solve the equations for the respective potentials in the metric tensor and for the nonlocal part of the energy explicitly by the superposition of monopoles.

The relevant length scales and parameters in our system are the following. We assume that initially we have a uniform distribution of particles contained in the box  $(0, L)^3$ . This property will not be conserved by the evolution but within the typical time scale particles remain in a box of order of size  $L$ .

We denote by  $\frac{1}{d^3}$  the number density of particles, such that  $d$  is the typical distance of one particle to its nearest neighbor, and we call  $\mathcal{R}$  the typical size of the radii of the particles. We are interested in the case that the  $A$ -phase has small volume fraction and hence we always assume that

$$\varepsilon := \frac{\mathcal{R}^3}{d^3} \ll 1. \quad (14)$$

It is well-known and it will also be apparent in the computations below that the crucial intrinsic length scale in diffusional interactions is the so-called screening length

$$L_{sc} = \left(\frac{d^3}{\mathcal{R}}\right)^{1/2}, \quad (15)$$

which describes the effective range of particle interactions. The following heuristic analysis shows that the leading order dynamics significantly differ, depending on whether  $L \ll L_{sc}$  or whether  $L \sim L_{sc}$ . Furthermore we denote by  $\mathcal{V}$  typical velocities.

### 2.2.1 The energy

In a first step we express the energy in terms of  $\{R_i, X_i\}_i$  which is trivial for the surface energy  $E_{surf}(\mathbf{Y}) = 4\pi \sum_i \frac{R_i^2}{2}$ , but also simple for the nonlocal energy.

Indeed, the solution of  $-\Delta\mu = \chi$ , is given by

$$\mu = \sum_i \mu_i,$$

where

$$\mu_i(x) = \begin{cases} -\frac{|x-X_i|^2}{6} + \frac{R_i^2}{2} & : \text{ in } B_{R_i}(X_i) \\ \frac{R_i^3}{3|x-X_i|} & : \text{ outside } B_{R_i}(X_i) \end{cases}. \quad (16)$$

Thus we find, using the mean-value theorem for  $\mu_j$  in  $B_{R_i}$  for  $j \neq i$ ,

$$\begin{aligned} E_{nl}(\mathbf{Y}) &= \frac{3}{2} \int_{\mathbb{R}^3} |\nabla\mu|^2 dx \\ &= \frac{3}{2} \sum_i \int_{B_{R_i}(X_i)} \mu dx \\ &= \frac{3}{2} \left( \sum_i \int_{B_{R_i}(X_i)} \mu_i dx + \sum_i \int_{B_{R_i}(X_i)} \sum_{j \neq i} \mu_j dx \right) \\ &= \frac{3}{2} \left( \sum_i \int_{B_{R_i}(X_i)} \mu_i dx + \sum_i \sum_{j \neq i} \frac{4\pi}{3} R_i^3 \mu_j(x_i) \right) \\ &= \frac{3}{2} \left( \frac{8\pi}{15} \sum_i R_i^5 + \frac{4\pi}{9} \sum_i \sum_{j \neq i} \frac{R_i^3 R_j^3}{|X_i - X_j|} \right) \\ &= 4\pi \left( \sum_i \frac{R_i^5}{5} + \frac{1}{6} \sum_i \sum_{j \neq i} \frac{R_i^3 R_j^3}{|X_i - X_j|} \right). \end{aligned} \quad (17)$$

Hence, the differential of the energy  $E = 4\pi \sum_i \frac{R_i^2}{2} + \gamma E_{nl}$  is given by

$$\begin{aligned} \frac{1}{4\pi} \langle DE(\mathbf{Y}), \tilde{\mathbf{Z}} \rangle &= \sum_i R_i \tilde{V}_i + \gamma \sum_i R_i^4 \tilde{V}_i + \gamma \sum_i \sum_{j \neq i} \frac{R_i^2 R_j^3}{|X_i - X_j|} \tilde{V}_i \\ &\quad - \frac{\gamma}{3} \sum_i \sum_{j \neq i} \frac{R_i^3 R_j^3}{|X_i - X_j|^2} \frac{(X_i - X_j)}{|X_i - X_j|} \cdot \tilde{\xi}_i. \end{aligned} \quad (18)$$

We can now compare the order of size of the different terms. First notice that in order that surface and nonlocal energy balance, the parameter  $\gamma$  has to be of size of order  $\mathcal{R}^{-3}$  which we assume from now on.

Furthermore, also in what follows, we approximate sums by the corresponding integral, i.e.  $\sum_i \frac{1}{|x-X_i|} \sim \frac{1}{d^3} \int_{B_L(0)} \frac{1}{|x|} \sim \frac{L^2}{d^3}$ , and we find that  $\sum_{j \neq i} \frac{R_i^3 R_j^3}{|X_i - X_j|}$  has size of order  $\mathcal{R}^6 \frac{L^2}{d^3}$ . This is smaller than  $\mathcal{R}^5$ , the order of size of  $R_i^5$ , if  $\frac{\mathcal{R}}{d^3} L^2 \ll 1$  or in other words, in view of (15), if  $L \ll L_{sc}$ .

Equivalently we can neglect the last two terms on the right hand side of (18) compared to the first two if  $L \ll L_{sc}$ . If  $L \sim L_{sc}$ , all terms are of the same order of size.

### 2.2.2 The metric tensor

In this section we address the metric tensor. Unfortunately, we cannot express the metric tensor completely explicitly in  $R_i, X_i$ , but we can estimate the single non-explicit term and we will see that it is not relevant in the regimes of interest.

We compute the metric tensor for given  $\mathbf{Z} = \{V_i, \xi_i\}_i$  solving the equations for the potential  $w = u + \phi$  respectively by the superposition of single particle solutions.

Recall that  $g_{\mathbf{Y}}(\mathbf{Z}, \mathbf{Z}) = \int_{\mathbb{R}^3} |\nabla w|^2 dx = \int_{\mathbb{R}^3} |\nabla u|^2 dx + 2 \int_{\mathbb{R}^3} \nabla u \cdot \nabla \phi dx + \int_{\mathbb{R}^3} |\nabla \phi|^2 dx$ , where  $u$  and  $\phi$  are given by (12).

One easily verifies that in the case of a single particle  $B_{R_i}(X_i)$  the solutions of problem (12) are given by

$$\begin{aligned} u_i(x) &= \begin{cases} -\frac{R_i^2 V_i}{|x - X_i|} & : |x - X_i| \geq R_i \\ -R_i V_i & : |x - X_i| \leq R_i \end{cases} \\ \phi_i(x) &= \begin{cases} -\frac{R_i^3}{|x - X_i|^3} (x - X_i) \cdot \xi_i & : |x - X_i| \geq R_i \\ -(x - X_i) \cdot \xi_i & : |x - X_i| \leq R_i \end{cases}. \end{aligned} \quad (19)$$

Hence, for a system with  $N$  particles the potentials are given by

$$u(x) := \sum_i u_i(x) \quad \text{and} \quad \phi(x) := \sum_i \phi_i(x).$$

We first observe

$$\begin{aligned} \int_{\mathbb{R}^3} |\nabla u|^2 dx &= \sum_i \int_{\mathbb{R}^3} |\nabla u_i|^2 dx + \sum_i \sum_{j \neq i} \int_{\mathbb{R}^3} \nabla u_i \cdot \nabla u_j dx \\ &= - \sum_i \int_{\partial B_{R_i}(X_i)} [\nabla u_i \cdot \vec{n}] u_i dS \\ &\quad - \sum_i \int_{\partial B_{R_i}(X_i)} [\nabla u_i \cdot \vec{n}] \sum_{j \neq i} u_j dS. \end{aligned} \quad (20)$$

Now,  $[\nabla u_i \cdot \vec{n}] = V_i$  is constant on  $\partial B_{R_i}(X_i)$  and  $u_j$  is harmonic in  $B_{R_i}(X_i)$ . Hence, the mean value theorem for harmonic functions implies that  $\int_{\partial B_{R_i}(X_i)} [\nabla u_i \cdot \vec{n}] \sum_{j \neq i} u_j dS = \sum_{j \neq i} V_i 4\pi R_i^2 u_j(X_i)$  and we arrive at

$$\int_{\mathbb{R}^3} |\nabla u|^2 dx = 4\pi \sum_i R_i^3 V_i^2 + 4\pi \sum_i \sum_{j \neq i} V_i V_j \frac{R_i^2 R_j^2}{|X_i - X_j|}. \quad (21)$$

Again we can compare the order of the first and second term in (21) respectively, as we did it for the energy in Section 2.2.1. Keeping in mind that the number of particles is of order  $\frac{L^3}{d^3}$ , we find that the first term is of size of order  $\frac{L^3}{d^3} \mathcal{R}^3 \mathcal{V}^2$ , where  $\mathcal{V}$  denotes the order of size of the velocities. Again approximating sums by integrals, the order of size

of the second term is  $\frac{L^3}{d^3} \mathcal{V}^2 \mathcal{R}^4 \frac{L^2}{d^3}$ . Hence, the first term dominates if and only if  $L^2 \ll \frac{d^3}{\mathcal{R}}$ , that is, again, if the box size is much smaller than the screening length.

Similarly as in (20) we compute

$$\begin{aligned}
\int_{\mathbb{R}^3} |\nabla \phi|^2 dx &= \sum_i \int_{\mathbb{R}^3} |\nabla \phi_i|^2 dx + \sum_i \sum_{j \neq i} \int_{\mathbb{R}^3} \nabla \phi_i \cdot \nabla \phi_j dx \\
&= - \sum_i \int_{\partial B_{R_i}(X_i)} [\nabla \phi_i \cdot \vec{n}] \phi_i dS \\
&\quad - \sum_i \int_{\partial B_{R_i}(X_i)} [\nabla \phi_i \cdot \vec{n}] \sum_{j \neq i} \phi_j dS \\
&= \sum_i 4\pi R_i^3 \int_{\partial B_{R_i}(X_i)} |\xi_i \cdot \vec{n}|^2 dS \\
&\quad - \sum_i \int_{\partial B_{R_i}(X_i)} \xi_i \cdot \vec{n} \sum_{j \neq i} \phi_j dS.
\end{aligned} \tag{22}$$

Here and in the following we use the notation  $\int_{\partial B_{R_i}} := \frac{1}{4\pi R_i^2} \int_{\partial B_{R_i}}$  for mean values. It is easily calculated, e.g. by using polar coordinates, that

$$\int_{\partial B_{R_i}(X_i)} |\xi_i \cdot \vec{n}|^2 dS = \int_{S^2} |\xi_i \cdot \vec{n}|^2 dS = \frac{1}{3} |\xi_i|^2$$

and thus

$$\int_{\mathbb{R}^3} |\nabla \phi|^2 ds = \frac{4\pi}{3} \sum_i R_i^3 |\xi_i|^2 - \sum_i \int_{\partial B_{R_i}(X_i)} \xi_i \cdot \vec{n} \sum_{j \neq i} \phi_j dS. \tag{23}$$

The second term is the one in the metric tensor which cannot be expressed explicitly in  $\{R_i, X_i\}$ . However, it turns out that it is of higher order than the second term in (21) and hence in particular also smaller than the diagonal terms. Indeed, the second term in (23) is of order  $\mathcal{V}^2 \frac{L^3}{d^3} \mathcal{R}^5 \frac{L}{d^3}$  and the ratio of this term and the second term in (21) is of order  $\frac{\mathcal{R}}{L} = \varepsilon^{1/3} \ll 1$ .

Finally we are going to argue that the mixed term  $\int_{\mathbb{R}^3} \nabla u \cdot \nabla \phi dx$  in the metric tensor is of higher order. Indeed, we find

$$\begin{aligned}
\int_{\mathbb{R}^3} \nabla u \cdot \nabla \phi dx &= \sum_i \int_{\mathbb{R}^3} \nabla u_i \cdot \nabla \phi dx \\
&= - \sum_i \int_{\partial B_{R_i}(X_i)} V_i \phi dS \\
&= - \sum_i V_i \int_{\partial B_{R_i}(X_i)} \sum_{j \neq i} \phi_j dS \\
&= - \sum_i \sum_{j \neq i} \frac{R_j^3 R_i^2}{|X_i - X_j|^3} V_i(X_i - X_j) \cdot \xi_j.
\end{aligned} \tag{24}$$

In the last equalities we used that  $\int_{\partial B_{R_i}(X_i)} \phi_i dS = -R_i \int_{\partial B_{R_i}(X_i)} \xi_i \cdot \vec{n} dS = 0$  and, as in the derivation of (21), that  $\phi_j$  is harmonic in  $B_{R_i}(x_i)$  for  $j \neq i$ . Now the order of the term can be estimated as  $\mathcal{V}^2 \frac{L^3}{d^3} \mathcal{R}^5 \frac{L}{d^3}$ . This is the same order as the off-diagonal term in (22) and can henceforth be neglected.

To summarize we obtain

$$g_{\mathbf{Y}}(\mathbf{Z}, \mathbf{Z}) = 4\pi \sum_i R_i^3 V_i^2 + 4\pi \sum_i R_i^3 \frac{1}{3} |\xi_i|^2 + \left( 4\pi \sum_i \sum_{j \neq i} \frac{R_i^2 R_j^2}{|X_i - X_j|} V_i V_j \right) \left( 1 + O(\varepsilon^{1/3}) \right). \quad (25)$$

and the diagonal terms dominate if  $L \ll L_{sc}$ .

## 2.3 Leading order approximations

We now set up an approximation of the gradient flow, keeping only the leading order terms in the energy and the metric tensor respectively. This will be the starting point for numerical simulations whose results we present in Section 4 below. As we have seen, there are two regimes of interest. The first one is the dilute case, where the system size is much smaller than the screening length.

### 2.3.1 Case I: $L \ll L_{sc}$

In case  $L \ll L_{sc}$  we obtain, in view of (17) and the subsequent discussion, that

$$E(\mathbf{Y}) \sim 4\pi \left( \sum_i \frac{R_i^2}{2} + \gamma \sum_i \frac{R_i^5}{5} \right), \quad (26)$$

whereas the metric tensor can be approximated due to (25) by

$$g_{\mathbf{Y}}(\mathbf{Z}, \mathbf{Z}) \sim 4\pi \sum_i R_i^3 \left( V_i^2 + \frac{1}{3} |\xi_i|^2 \right).$$

The gradient flow equation  $g_{\mathbf{Y}}(\mathbf{Z}, \tilde{\mathbf{Z}}) + \langle DE(\mathbf{Y}), \tilde{\mathbf{Z}} \rangle = 0$  reads as

$$\sum_i R_i^3 \left( V_i \tilde{V}_i + \frac{1}{3} \xi_i \cdot \tilde{\xi}_i \right) + \sum_i R_i \tilde{V}_i + \gamma \sum_i R_i^4 \tilde{V}_i = 0$$

for all  $\{\tilde{V}_i, \tilde{\xi}_i\}$  in the tangent space. This is equivalent to

$$\sum_i R_i^3 \left( V_i \tilde{V}_i + \frac{1}{3} \xi_i \cdot \tilde{\xi}_i \right) + \sum_i R_i \tilde{V}_i + \gamma \sum_i R_i^4 \tilde{V}_i = \lambda \sum_i R_i^2 \tilde{V}_i$$

for all  $\{\tilde{V}_i, \tilde{\xi}_i\} \in \mathbb{R}^{4N}$  and where  $\lambda$  is a Lagrange multiplier, which ensures  $\sum_i R_i^2 V_i = 0$ .

Consequently we obtain for the direction of steepest descent that

$$V_i = \frac{1}{R_i^2}(\lambda R_i - 1 - \gamma R_i^3) \quad \text{and} \quad \xi_i = 0, \quad (27)$$

where

$$\lambda = \frac{\sum_{i:R_i>0} 1 + \gamma \frac{3\rho}{4\pi}}{\sum_i R_i}. \quad (28)$$

### 2.3.2 Case II: $L \sim L_{sc}$

With the same procedure as above we obtain, using (18) and (25), that  $V_i$  solves the linear system of equations

$$R_i^2 V_i + R_i \sum_{j \neq i} \frac{R_j^2}{|X_i - X_j|} V_j + 1 + \gamma R_i^3 + \gamma R_i \sum_{j \neq i} \frac{R_j^3}{|X_i - X_j|} = \lambda R_i, \quad (29)$$

where  $\lambda$  is such that  $\sum_i R_i^2 V_i = 0$  and we obtain a nontrivial evolution equation for the centers, namely

$$\xi_i = \gamma \sum_{j \neq i} \frac{R_j^3}{|X_i - X_j|^3} (X_i - X_j). \quad (30)$$

## 2.4 Mean-field models

In this section we derive mean-field models which arise if one passes from the discrete setting of finitely many particles to a description with densities. Our derivation is purely formal and starts from (27) and (29)-(30) respectively. A rigorous derivation from the full model in the spirit of [9] seems feasible under some assumptions on the distribution of particles, this is however not within the scope of this paper.

For the derivation of mean-field models we need to go over to suitably rescaled variables. First we recall the relevant parameters and length scales in our system. We denote by  $N$  the total number of particles, by  $\frac{1}{d^3}$  the number density and  $\mathcal{R}$  denotes the typical particle radius. Our system size, that is the area covered with particles, is then  $L^3 \sim N d^3$ . The crucial intrinsic length scale is the screening length  $L_{sc} \sim \left(\frac{d^3}{\mathcal{R}}\right)^{1/2}$ . Note that these quantities are in general time dependent. As introduced here they refer to the initial configuration and we derive the mean-field models for finite times in which these length scales remain of the same order.

Recall also that in order to balance surface and nonlocal energy our parameter  $\gamma$  must be of order  $\mathcal{R}^{-3}$ . Hence, we set from now on

$$\tilde{\gamma} := \gamma \mathcal{R}^{-3}. \quad (31)$$

### 2.4.1 Case I: $L \ll L_{sc}$

We start with the easy case  $L \ll L_{sc}$ . In view of (27) we measure the time in which radii change in units of  $\mathcal{R}^3$ , that is we introduce the new time scale  $\tau = t/\mathcal{R}^3$ . Since  $\xi_i = 0$  in the dilute regime, it suffices to consider the distribution of particle radii. Let

$$r_i(\tau) = \frac{R_i(t)}{\mathcal{R}}, \quad v_i := \mathcal{R}^2 V_i \quad (32)$$

and define

$$\int \zeta \nu_\tau(dr) := \frac{1}{N} \sum_i \zeta(r_i), \quad (33)$$

where  $\zeta \in C_0^\infty((0, \infty))$ . Then, using (27), we find

$$\begin{aligned} \frac{d}{d\tau} \int \zeta \nu_t(dr) &= \frac{1}{N} \sum_i \partial_r \zeta v_i \\ &= \frac{1}{N} \sum_i \partial_r \zeta \frac{1}{r_i^2} (\tilde{\lambda} r_i - 1 - \tilde{\gamma} r_i^3) \\ &= \int \partial_r \zeta \frac{1}{r^2} (\tilde{\lambda} r - 1 - \tilde{\gamma} r^3) \nu_\tau(dr), \end{aligned} \quad (34)$$

where  $\tilde{\lambda} = \lambda \mathcal{R}$  is such that  $\int r^3 \nu_t(dr) \equiv \frac{3\rho}{4\pi N} =: \tilde{\rho}$ . Equation (34) just means that  $\nu_t$  satisfies

$$\partial_\tau \nu_\tau + \partial_r \left( \frac{1}{r^2} (\tilde{\lambda} r - 1 - \tilde{\gamma} r^3) \nu_\tau \right) = 0 \quad (35)$$

with

$$\tilde{\lambda}(\tau) = \frac{\int \nu_\tau(dr) + \tilde{\gamma} \tilde{\rho}}{\int r \nu_\tau(dr)} \quad (36)$$

in the sense of distributions.

For  $\tilde{\gamma} = 0$  we recover the LSW-theory for coarsening of particles. For  $\tilde{\gamma} > 0$  the additional term  $\tilde{\gamma} \sum_i \frac{R_i^5}{5}$  in the energy prevents coarsening and hence the long-time behavior of (35) is different from the one for  $\tilde{\gamma} = 0$ . Indeed, while the energy (26) together with the volume constraint has no stationary point for  $\tilde{\gamma} = 0$ , we will see in Section 3 below, that (26) has a unique global minimizer for  $\tilde{\gamma} > 0$  which is also the only stationary point (with respect to an appropriate topology).

### 2.4.2 Case II: $L \sim L_{sc}$

We assume now that  $L \sim L_{sc} = \left(\frac{d^3}{\mathcal{R}}\right)^{1/2}$ . In addition to  $r_i$  and  $v_i$  as in (32) we also introduce

$$x_i(\tau) := \frac{X_i(t)}{L_{sc}} \quad \text{and} \quad \psi_i := \frac{d^3}{L_{sc}} \xi_i. \quad (37)$$

Now we define the joint distribution of particle centers and radii via

$$\int \zeta \nu_\tau(dx dr) := \frac{1}{N} \sum_i \zeta(x_i, r_i) \quad (38)$$

for  $\zeta \in C_0^\infty(\mathbb{R}^3 \times (0, \infty))$ . We are going to derive that  $\nu_t$  satisfies the following system of equations in a distributional sense:

$$\partial_\tau \nu_\tau + \partial_r \left( \frac{1}{r^2} (r\bar{u} - 1 - \tilde{\gamma}(r^3 + rK(x))) \nu_\tau \right) + \varepsilon \tilde{\gamma} \operatorname{div}_x (-\nabla K(x) \nu_\tau) = 0, \quad (39)$$

where  $\varepsilon$  is the volume fraction (recall (14)) and

$$K(x) = \int \frac{s^3}{|x-y|} \nu_\tau(dy ds) \quad (40)$$

(notice that the integral is finite since  $\nu_\tau$  has finite support in the  $x$ -variable) and  $\bar{u} = \bar{u}(x, \tau)$  satisfies for each  $\tau$

$$-\frac{1}{4\pi} \Delta_x \bar{u} + \bar{u} \int_0^\infty r \nu_\tau(dr) - \int_0^\infty \nu_\tau(dr) - \tilde{\gamma} \left( \int_0^\infty r^3 \nu_\tau(dr) + K(x) \int_0^\infty r \nu_\tau(dr) \right) = 0 \quad (41)$$

in  $\mathbb{R}^3$ .

Indeed, we first recall (37), to find

$$\frac{d}{d\tau} \int \zeta \nu_\tau(dx dr) = \frac{1}{N} \sum_i (\varepsilon \nabla \zeta \cdot \psi_i + \partial_r \zeta v_i). \quad (42)$$

Equation (30) gives

$$\begin{aligned} \psi_i &= \tilde{\gamma} \frac{d^3}{L_{sc}} \sum_{j \neq i} \frac{R_j^3}{\mathcal{R}^3} \frac{X_i - X_j}{|X_i - X_j|^3} \\ &= \tilde{\gamma} \frac{d^3}{L_{sc}^3} \sum_{j \neq i} r_j^3 \frac{x_i - x_j}{|x_i - x_j|^3} \\ &= \tilde{\gamma} \frac{1}{N} \sum_{j \neq i} r_j^3 \frac{x_i - x_j}{|x_i - x_j|^3} \\ &= -\tilde{\gamma} \nabla K(x_i). \end{aligned} \quad (43)$$

In order to express  $v_i$  we introduce (neglecting in the notation the dependence on  $t$ )

$$-\bar{u}(x) := \mathcal{R} \left( \sum_{j \neq i} \frac{R_j^2 V_j}{|x - X_j|} - \lambda \right) = \mathcal{R} \left( \frac{1}{L_{sc}} \sum_{j \neq i} \frac{r_j^2 v_j}{|x - x_j|} - \lambda \right). \quad (44)$$

Then (29) reads

$$\begin{aligned} R_i^2 V_i &= \frac{R_i \bar{u}(x_i)}{\mathcal{R}} - 1 - \gamma \left( R_i^3 + R_i \frac{\mathcal{R}}{L_{sc}} \sum_{k \neq i} \frac{R_k^3}{|x - x_k|} \right) \\ &= R_i \bar{u}(x_i) - 1 - \tilde{\gamma} \left( r_i^3 + r_i K(x_i) \right), \end{aligned} \quad (45)$$

where we used (40) in the last step as well as the fact  $\frac{\mathcal{R}N}{L_{sc}} = 1$  which is due to  $L = L_{sc}$ . Inserting (45) into (44) we obtain

$$\begin{aligned} -\bar{u}(x) &= \frac{\mathcal{R}}{L_{sc}} \sum_{j \neq i} \frac{r_j \bar{u}(x_j) - 1 - \tilde{\gamma}(r_j^3 + r_j K(x_j))}{|x - x_j|} - \lambda \mathcal{R} \\ &= \int \frac{r \bar{u}(y) - 1 - \tilde{\gamma}(r^3 + r K(y))}{|x - y|} \nu_\tau(dy dr) - \lambda \mathcal{R}. \end{aligned}$$

If we take the Laplacian in the last equation we obtain (41). Finally, (39) follows from (42), (43) and (45).

### 3 Stationary points of the energy

In this section we investigate the stationary states of the energies. Since we are interested in configurations with a large number of particles, we consider the continuous case. As we will argue later, in our setting stationary points only exist in the dilute case so we first concentrate on this. For notational convenience we rename  $\tilde{\rho}$  and  $\tilde{\gamma}$  by  $\rho$  and  $\gamma$  again. Thus, let  $\nu$  be a measure on  $(0, \infty)$  so that

$$\rho = \frac{4\pi}{3} \int_0^\infty r^3 \nu(dr) \quad (46)$$

is fixed. The energy of  $\nu$  is

$$E(\nu) = 4\pi \int \left( \frac{r^2}{2} + \gamma \frac{r^5}{5} \right) \nu(dr). \quad (47)$$

**Lemma 3.1.** *Among measures  $\nu$  with the fixed volume  $\rho$  the energy  $E$  is minimized at  $\nu = \frac{3\rho}{4\pi r_*^3} \delta_{r_*}$ , where  $r_* = (\frac{5}{4\gamma})^{1/3}$ .*

*Proof.* Let  $\mu$  be a measure so that

$$\mu(dr) = r^3 \nu(dr). \quad (48)$$

Then

$$E(\nu) = 4\pi \int \left( \frac{1}{2r} + \gamma \frac{r^2}{5} \right) \mu(dr)$$

Since the integrand is convex, by Jensen's inequality

$$E(\nu) \geq 3\rho \left( \frac{1}{2\bar{r}} + \gamma \frac{\bar{r}^2}{5} \right) \quad (49)$$

where  $\bar{r} = \frac{4\pi}{3\rho} \int r \mu(dr)$  is the average of  $r$  under  $\mu$ . Note that equality in (49) holds only when  $\mu = \frac{3\rho}{4\pi} \delta_{\bar{r}}$ . In this case  $\nu = \frac{3\rho}{4\pi \bar{r}^3} \delta_{\bar{r}}$ . So it suffices to minimize  $E$  among such measures and, since

$$E\left(\frac{\rho}{\bar{r}^3} \delta_{\bar{r}}\right) = 3\frac{\rho}{\bar{r}^3} \left( \frac{\bar{r}^2}{2} + \gamma \frac{\bar{r}^5}{5} \right) = 3\rho \left( \frac{1}{2\bar{r}} + \gamma \frac{\bar{r}^2}{5} \right) \quad (50)$$

is convex in  $\bar{r}$ ,  $E$  is minimized at

$$\frac{3\rho}{4\pi r_*^3} \delta_{r_*}, \quad \text{with} \quad r_* = \left(\frac{5}{4\gamma}\right)^{1/3} \quad (51)$$

□

Next we investigate stationary points of  $E$ . The notion of stationary points depends on the variations and hence the topology one uses in the space of measure. The coarsest topology is the one induced by the Wasserstein distance, which metrizes the weak topology of measures. In one dimension the Wasserstein distance is easy to compute. Let

$$Z_1(r) = \nu_1([r, \infty)), \quad Z_2(r) = \nu_2([r, \infty)) \quad (52)$$

be the radius distributions of the measures  $\nu_1$  and  $\nu_2$  and denote by  $r_1(z), r_2(z)$  their right-continuous inverses. The  $L^p$ -Wasserstein distance between  $\nu_1$  and  $\nu_2$  is given by

$$\rho(\nu_1, \nu_2) := \|r_1 - r_2\|_p = \left( \int_0^\infty |r_1(z) - r_2(z)|^p dz \right)^{1/p}. \quad (53)$$

In the next lemma we show that the only stationary point of the energy with respect to the topology induced by the Wasserstein distance is the global minimizer identified in Lemma 3.1.

**Lemma 3.2.** *Let  $\nu$  be a stationary point of  $E$  with respect to the topology induced by (53). Then  $\nu = \frac{3\rho}{4\pi r_*^3} \delta_{r_*}$  and  $r_* = \left(\frac{5}{4\gamma}\right)^{1/3}$ .*

*Proof.* Let  $\nu$  be a stationary point of  $E$  and  $r = r(z)$  the right-continuous inverse of its distribution function as described above. We do not assume that  $\nu$  is a finite measure, hence  $r$  might not have finite support. In terms of  $r$  the energy is given by

$$E(\nu) = 4\pi \int_0^\infty \frac{r^2(z)}{2} + \gamma \frac{r^5(z)}{5} dz =: \hat{E}(r).$$

The constraint  $\frac{4\pi}{3} \int r^3 \nu(dr) = \rho$  corresponds to  $\frac{4\pi}{3} \int r^3(z) dz = \rho$ . We consider now so called inner variations, that is we consider  $r^\varepsilon(z) := r(z + \varepsilon\eta(z))$ , where  $\eta \in C_0^\infty((0, \infty))$  is such that  $\frac{4\pi}{3} \int_0^\infty r^\varepsilon(z) dz = \rho$ . We find

$$\begin{aligned} \frac{d}{d\varepsilon} \hat{E}(r^\varepsilon)|_{\varepsilon=0} &= \frac{d}{d\varepsilon}|_{\varepsilon=0} \int_0^\infty \left( \frac{r^{\varepsilon 2}}{2} + \gamma \frac{r^{\varepsilon 5}}{5} \right) dz \\ &= - \int_0^\infty \left( \frac{r^2}{2} + \gamma \frac{r^5}{5} \right) \eta'(z) dz. \end{aligned}$$

Furthermore, the volume constraint  $\frac{4\pi}{3} \int_0^\infty r^{\varepsilon 3}(z) dz = \rho$  implies similarly that  $\int_0^\infty r^3 \eta'(z) dz = 0$ . Thus, in summary we find that

$$\int_0^\infty \left( \frac{r^2}{2} + \gamma \frac{r^5}{5} - \lambda r^3 \right) \psi'(z) dz = 0 \quad (54)$$

for all  $\psi \in C_0^\infty((0, \infty))$  and for some  $\lambda \in \mathbb{R}$ . Let  $\{z_i\}, i \in I \subset \mathbb{N}$ , be the set of discontinuity points of  $r$  (which is at most a countable set, since  $r$  is decreasing). With this notation we deduce from (54) after an integration by parts that

$$\int_0^\infty (r + \gamma r^4 - 3\lambda r^3)\psi(z) dz + \sum_{i \in I} \left[ \left( \frac{r^2}{2} + \gamma \frac{r^5}{5} - \lambda r^3 \right)(z_i) - \lim_{z \rightarrow z_i, z < z_i} \left( \frac{r^2}{2} + \gamma \frac{r^5}{5} - \lambda r^3 \right)(z) \right] \psi(z_i) = 0$$

for all  $\psi \in C_0^\infty((0, \infty))$ . It follows that  $r$  has to be piecewise constant, say  $r(z) \equiv r_i \in [z_{i-1}, z_i)$  (with the convention that  $z_0 = 0$ ), and  $r_i$  must be a zero of  $f(r) := r + \gamma r^4 - 3\lambda r^2$  for some  $\lambda \in \mathbb{R}$ . Second, we find

$$\frac{r_i^2}{2} + \gamma \frac{r_i^5}{5} - \lambda r_i^3 = \frac{r_{i-1}^2}{2} + \gamma \frac{r_{i-1}^5}{5} - \lambda r_{i-1}^3$$

for all  $i \in I$ . A simple calculation shows that this can only be true if  $I = \{1\}$  and  $r_1 = r_* = \left(\frac{5}{4\gamma}\right)^{1/3}$  and  $r_2 = 0$ . The point  $z_1$ , where  $r$  jumps is determined by the volume constraint and hence given as  $z_1 = \frac{3\rho}{4\pi r_*^3}$ .  $\square$

**Remark 3.3.** (*The inhomogeneous case*)

It is in principle a very interesting question, how in the case of  $L \sim L_{sc}$  the additional inhomogeneous term in the energy, namely as

$$\frac{1}{N^2} \sum_i r_i^3 \sum_{j \neq i} \frac{r_j^3}{|x_i - x_j|} = \int r^3 K(x) \nu(dx dr),$$

changes the configuration of stationary points. However, in our case, there are no stationary states. This is due to the somewhat artificial setting, where we set particles in a bounded domain but solve the equations for the corresponding potentials in full space. This implies equation (30) for the evolution of particle centers from which we easily see, that particles lying on the boundary of our “cloud” of particles will be driven further outwards.

If instead we would confine particles and their corresponding potentials to a finite domain and pose periodic or Neumann boundary conditions we would obtain similar formulas for our approximate gradient flow equations and the mean-field models, but  $\frac{1}{|x|}$  would be replaced by the corresponding Green’s function. Then stationary states would be characterized by  $K \equiv \text{const}$ , which would imply a regular spacing of the particles. Once  $K$  is constant, the term  $\int r^3 K \nu(dx dr)$  is also constant due to the volume constraint. The remaining discussion of stationary points is then analogous to the dilute case.

From the discussion in the mean-field theory, Section 2.4.2, we know that the particle centers move on a slower time scale  $d^3$  than the particle radii, which change on a time scale of order  $\mathcal{R}^3$ . Consequently, in our simulations, the movement of particles is almost negligible compared to the evolution of the radii.

**Remark 3.4.** (*The discrete setting*)

Naturally, the discrete case is somewhat different from the continuous one, since the number is discrete and we cannot reach any arbitrary fraction of particles. As argued in Remark 3.3 above, we can concentrate on the dilute case (27).

Let us first consider the situation from the point of view of the evolution. Our initial configuration consists of  $N$  particles with total volume  $\rho = \sum_i \frac{4\pi}{3} R_i^3 \sim N \frac{4\pi \mathcal{R}^3}{3}$ . Since during our evolution particles can only vanish, we consider stationary states with  $N_1 \leq N$  particles. For any given  $N_1$  there is a family of stationary states. First there is the trivial one, that is  $R_i \equiv \hat{r}$  for all  $i$  and  $\hat{r} = \frac{3\rho}{4\pi N_1}$ . However, due to the discreteness of the problem there are now also stationary states with two different sizes of particles. For that let  $\sigma := \frac{N_2}{N_1} \in (0, 1]$ , where  $N_2$  will be the number of particles with one radius  $r_1$ , whereas  $N_1 - N_2$  will be the number of particles with another radius  $r_2$ . In view of (27) stationary states of the desired form are given by radii which are zeros of the function  $f(r) := 1 + \gamma r^3 - \lambda r$  for some  $\lambda \in \mathbb{R}$ . There can be at most two different radii for which this is satisfied. We denote them by  $r_1$  and  $r_2$ . To say that  $r_1$  and  $r_2$  are zeros of the function  $f$  for some  $\lambda$  is equivalent to requiring that  $\frac{1}{r_1} + \gamma r_1^2 = \frac{1}{r_2} + \gamma r_2^2$  holds true. In order to satisfy the volume constraint, we must have  $\sigma r_1^3 + (1 - \sigma)r_2^3 = \frac{3\rho}{4\pi N_1} =: \beta$ . Using the last equation to express  $r_2$  by  $r_1$  we find that  $r_2^3 = \frac{\beta - \sigma r_1^3}{1 - \sigma}$ . Now the corresponding  $r_1$  is determined as a zero of  $g(r) := \frac{1}{r} + \gamma r^2 - \left(\frac{1 - \sigma}{\beta - \sigma r^3}\right)^{1/3} - \gamma \left(\frac{\beta - \sigma r^3}{1 - \sigma}\right)^{2/3}$ . Since  $\lim_{r \rightarrow 0} g(r) = +\infty$  and  $\lim_{r \rightarrow \sigma^{-1/3}} g(r) = -\infty$  there is at least one solution. Thus we have a whole set of stationary states for given  $N_1 \leq N$  which consist of two different sizes of particles. Due to the convexity of the energy they have higher energy than the stationary state where only one size is present and the size is given by  $\hat{r} = \frac{3\rho}{4\pi N_1}$ . This is true for fixed  $N_1$ . Of course, depending on the choice of parameters, it might be that a stationary state with two different sizes for one  $N_1$  has lower energy than the trivial stationary state for a different given number of particles.

## 4 Simulations

For numerical simulation it is convenient to re-formulate (27) and (29) in terms of particle volumes and their velocities instead of radii. This has the advantage that the constraint of volume conservation becomes linear. For that let  $W_i := R_i^3$  and  $\omega_i := \frac{d}{dt} W_i$ . The equations then read

$$\omega_i = 3(\lambda R_i - 1 - \gamma R_i^3) \quad \text{and} \quad \xi_i = 0 \quad (55)$$

with  $\lambda$  as in (28) in the dilute case, and

$$\begin{aligned} \omega_i + R_i \sum_{j \neq i} \frac{\omega_j}{|X_i - X_j|} + \lambda &= -3 - 3\gamma R_i^3 - 3\gamma R_i \sum_{j \neq i} \frac{R_j^3}{|X_i - X_j|}, \\ \xi_i &= \gamma \sum_{j \neq i} \frac{R_j^3}{|X_i - X_j|} (X_i - X_j) \end{aligned} \tag{56}$$

in case  $L \sim L_{sc}$ .

To simulate the behavior of our gradient flow model with these equations we set up a simple numerical scheme consisting of an Euler predictor and a trapezoidal rule corrector step. The latter is also used as error indicator and to determine – beside the influence of vanishing particles – a suitable step size. Particles are removed when they become too small, i.e. if  $W_i < \varepsilon \sum W_i / N$  where  $N$  denotes the current number of particles and  $\varepsilon$  is a user-defined tolerance. Under no circumstances we allow particle volumes to become negative.

At each time step the velocities of particle midpoints and volumes are computed via (55) and (56), respectively. While this is not much work in the first case, we have to solve a symmetric, indefinite, and dense linear system of size  $N + 1$ . in the second case. Due to its potential structure, however, the product of the system matrix with an arbitrary vector can be computed in almost linear time by means of the Fast Multipole Method [7, 8]. This and the approximate weak diagonal dominance of the matrix enable us to efficiently apply a Krylov subspace method to solve (56) for large systems.

We start our simulations with a number of particles distributed regularly on a mesh in some box  $[0, L]^3$ . From the mesh size and (15) we obtain the value of the initial mean or typical radius in order that  $L = L_{sc}$  is approximately fulfilled. We simulate the dilute and the full problem with the same radius distribution in order to be able to compare the results.

#### 4.1 Case I: $L \ll L_{sc}$

For any distribution of radii which we consider in our simulations, uniformly or normally distributed in some interval about the initial mean radius or special as stated below, the system reaches a stationary state. As expected from Remark 3.4 this final state is characterized by either all particles having (almost) the same size or one of two radii with the condition stated there. The latter case, however, only appears when we already start the simulation with such a particle configuration; in all other cases we end in a stationary state concentrated in one size.

However, the computed stationary state is not the global minimizer derived in Section 3, which, of course, might be infeasible due to the volume constraint and integer number of particles, but in general one cannot even say that it is close to or approaches it when

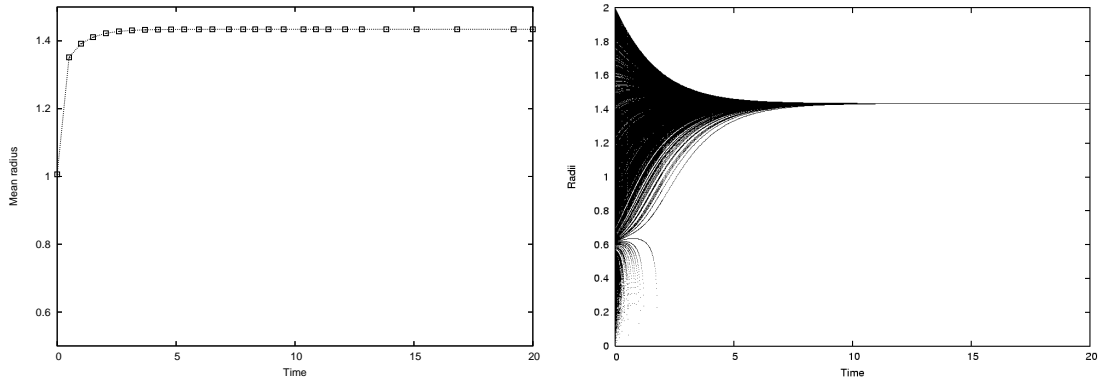


Figure 1: Example for an evolution of mean radius and all particle radii in the dilute case.

initial $N$	initial radii distribution	$(5/4\gamma)^{1/3}$	final radius	final $N$
1000	uniformly in $(0, 2)$	1.365	1.434	690
1000	uniformly in $(0.5, 1.5)$	1.365	1.202	742
1000	normally in $(0, 2)$	1.365	1.197	768
1000	normally in $(0.5, 1.5)$	1.365	1.115	846
2197	uniformly in $(0, 0.88)$	0.599	0.628	1529
4096	uniformly in $(0, 0.432)$	0.202	0.305	2866

Table 1: Results of simulated particle systems all within the same parameter region, but different radii distribution.

the number of particles grows. In fact, the computed state and its difference from the predicted minimizer of the continuous case in terms of the final radius depend on the actual distribution of the radii, as can be seen in Figure 1 and Table 1.

#### 4.2 Case II: $L \sim L_{sc}$

As expected, the evolution of the full problem does not reach a stationary state, i.e. a state in which all velocities are identically zero, since particles drift out of the box. But the following two observations can be made, as can be seen for instance in Figure 2. First of all even though drifting can occur, its influence on energy minimizing is distinguishable from that of radii evolution and – as already stated in Remark 3.3 – can be neglected in case that the actual value of  $L_{sc}$  is not much smaller than the box size. Secondly and more important, one can see that the total energy in principle tends towards a stationary value, as does the mean particle radius. However, the final mean radius is in general not equal to that from the same initial configuration evolving under the dilute equations. Another difference is that in the full problem the particles do not tend to have equal size. Instead, after a phase of vanishing and approaching it, all remaining particles have radii in some interval about the final mean radius which is smaller than the initial radii

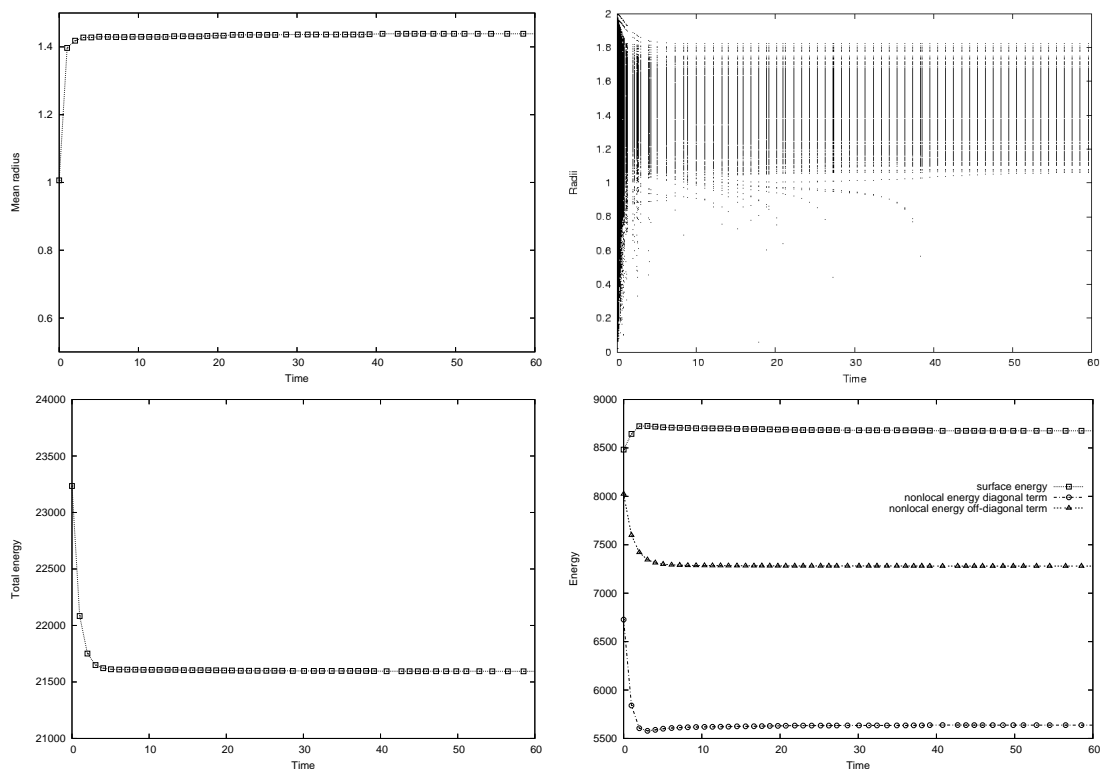


Figure 2: Evolution of mean radius, particle radii and energy in the full problem; compare with Figure 1 where the same system in the dilute case is shown.

interval, but whose size again seems to depend on the actual initial distribution.

**Acknowledgments.** The authors gratefully acknowledge support through the Humboldt University and the DFG Priority Program 1095 “Analysis, Modeling and Simulation of Multiscale Problems” .

## References

- [1] N. Alikakos and G. Fusco. Ostwald ripening for dilute systems under quasistationary dynamics. *Comm. Math. Phys.*, 238(3):429-479, 2003.
- [2] X. Chen. The Hele-Shaw problem and area-preserving curve shortening motion. *Arch. Rat. Mech. Anal.*, 123:117-151, 1993.
- [3] X. Chen, X. Hong and F. Yi. Existence, uniqueness and regularity of solutions of the Mullins-Sekerka problem. *Comm. PDE*, 21:1705-1727, 1996.

- [4] R. Choksi. Scaling laws in microphase separation of diblock copolymers. *J. Nonlinear Sci.*, 11(3):223–236, 2001.
- [5] S. Dai and R. L. Pego. On the monopole approximation of the Mullins-Sekerka model. Preprint, 2005.
- [6] J. Escher and G. Simonett. A center manifold analysis for the Mullins-Sekerka model. *J. Differential Equations*, 143:267-292, 1998.
- [7] L. Greengard. *The Rapid Evaluation of Potential Fields in Particle Systems*. MIT Press, Cambridge, Massachusetts, 1987.
- [8] L. Greengard and V. Rokhlin. A new version of the fast multipole method for the Laplace equation in three dimensions. *Acta Numerica*, 6:229–269, 1997.
- [9] B. Niethammer and F. Otto. Ostwald Ripening: The screening length revisited. *Calc. Var. and PDE*, 13 1:33–68, 2001.
- [10] Y. Nishiura and I. Ohnishi. Some mathematical aspects of the microphase separation in diblock copolymers. *Physica D*, 84(1-2):31–39, 1995.
- [11] T. Ohta and K. Kawasaki. Equilibrium morphology of block copolymer melts. *Macromolecules*, 19(10):2621–2632, 1986.
- [12] X. Ren and J. Wei. On the multiplicity of solutions of two nonlocal variational problems. *SIAM J. Math. Anal.*, 31(4):909–924, 2000.
- [13] X. Ren and J. Wei. Spherical solutions to a nonlocal free boundary problem from diblock copolymer morphology. *SIAM J. Math. Anal.*, to appear.